Available online at www.sciencedirect.com
SCIENCE DIRECT®
Catalysis Today 89 (2004) 67–74
CATALYSIS TODAY
www.elsevier.com/locate/cattod

Dissociation of vibrationally excited methane on Ni catalyst Part 2. Process diagnostics by emission spectroscopy

Tomohiro Nozaki*, Nahoko Muto, Shigeru Kadio, Ken Okazaki

Department of Mechanical and Control Engineering, Tokyo Institute of Technology, 2-12-1 O-okayama, Meguro-ku, Tokyo 152-8552, Japan

Abstract

Barrier discharge enhanced catalyst bed (BEC) reactor was developed for methane steam reforming. Synergistic effect between barrier discharge and Ni/SiO_2 catalyst was clearly observed when bed temperature exceeded 400 °C, energy cost and energy efficiency achieved 134 MJ/kg H_2 and 26%, respectively. This paper concentrates on two-temperature analysis of BEC reactor for better understanding of reaction mechanism. Catalyst bed temperature and plasma gas temperature were separately analyzed by emission spectroscopy of rotational band of $CH(A^2\Delta)$. Gas temperature distribution in packed-bed reactor was also estimated by using empirical correlations, and compared to spectroscopic data. Even though plasma gas temperature reached 400–500 °C, synergistic effect was not observed when catalyst bed temperature was below 400 °C. On the other hand, thermal reforming reaction was dominated over barrier discharges if the bed temperature exceeded 700 °C. As key radical species, reactivity of vibrationally excited methane is discussed based on vibrational temperature of $CH(A^2\Delta)$. Vibrational temperature was significantly increased in the presence of nickel catalyst, showing increased reactivity of vibrationally excited species.

Keywords: Steam reforming reaction; Barrier discharge enhanced catalyst bed; Methane

1. Introduction

Barrier discharge enhanced catalytic reforming of methane achieved great improvement of energy cost and energy efficiency. Methane conversion largely exceeded equilibrium conversion between 400 and 600 °C. On the other hand, product selectively tended to follow equilibrium composition at given temperature. Vibrational methane molecule at stretching mode (0.36 eV) is 1600 times more reactive on clean nickel surface than those at ground state molecule [1]. As a result, vibrational methane increased dissociative chemisorption on nickel catalyst. Computer simulation performed by authors [2] also supports reaction enhancement via vibrational methane and resulting plasma–catalyst synergistic effect. In order to make sure reactivity of vibrationally excited methane, we performed spectroscopic measurement for rotational and vibrational state of excited $CH(A^2\Delta)$ radical. Rotational temperature allows in situ measurement of gas kinetic temperature from emission region where various chemical and electronic processes take place. Not only bed temperature, but also plasma gas temperature was individually identified and discussed in detail at given conditions. Vibrational state of $CH(A^2\Delta)$ was also analyzed in BEC reactor with/without nickel catalyst. Reaction mechanism involving vibrationally excited methane is discussed with vibrational temperature of $CH(A^2\Delta)$.

2. Reaction scheme

According to Juurlink et al. [1], sticking probability of vibrationally excited methane on clean nickel surface increases one to two orders of magnitude larger than ground state molecule, thus promoting dissociative chemisorption of methane [3,4]. Fig. 1 schematically shows general aspects of catalytic reaction that consists of three different stages. In the first stage, vibrational methane generated by electron impact increases chemisorption on nickel surface at lower temperature. Ground state molecule also absorbed on nickel surface, but sticking coefficient is one to two orders of magnitude smaller than those at vibrational state. Those molecules would then dissociate and react with other

* Corresponding author. Tel.: +81-3-5734-2179; fax: +81-3-5734-2893.
E-mail address: tnozaki@mech.titech.ac.jp (T. Nozaki).

0920-5861/$ – see front matter © 2003 Elsevier B.V. All rights reserved.
doi:10.1016/j.cattod.2003.11.039

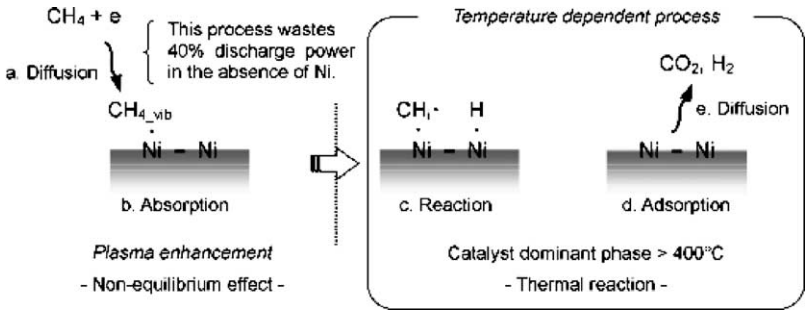

Fig. 1. Reaction scheme in plasma enhanced catalytic reaction.

molecules (second stage). Final products such as hydrogen and carbon monoxide will be then released from catalyst surface (third stage). Plasma plays an important role in the first stage to improve methane chemisorption, and then effectively increases methane conversion at lower temperature; methane conversion exceeded chemical equilibrium at given temperature. On the other hand, in the second and third stages, product selectivity relies strongly on catalytic reaction on nickel surface. Reforming reaction proceeds independently of barrier discharges if catalyst temperature is maintained at a certain level, and product selectivity tended to follow chemical equilibrium with increasing catalyst temperature. In order to investigate suggested reaction scheme, catalyst bed temperature, rotational temperature, and vibrational temperature was independently analyzed based on emission spectroscopy of CH($A^2\Delta$).

3. Experimental

Fig. 2 shows BEC reactor and optical measurement set-up. The reactor consists of glass tube (6 mm i.d.) with stainless steel wire electrode located at the center. The glass tube was filled with 1.2 mm SiO_2 pellet (with/without 3 wt.% Ni). This reactor was embedded in a copper block that was used as ground electrode as well as heat reservoir to maintain uniform and stable temperature condition. High voltage sine wave was applied between wire electrode and copper electrode (76 kHz). The copper block was equipped with electric heater and thermocouple. Methane conversion and hydrogen selectivity was monitored to make sure whether steam reforming took place properly. Details for gas analysis is described in separate paper [2].

Table 1
Experimental conditions

Total flow rate	26 sccm
H_2O/CH_4	2:1 (CH_4 content 33%)
Electrode temperature	200, 400, 600 °C
Pressure	101.3 kPa
Frequency	76 kHz
Pellet diameter	1.2 mm
Material	SiO_2 with/without 3 wt.% Ni
Power	35 W

Emission spectroscopy of rotational band of CH ($A^2\Delta \rightarrow X^2\Pi$, 431.5 nm) was performed to determine gas kinetic temperature in the corresponding emission region. Emission from barrier discharge was recorded by intensified charge coupled device (ICCD) camera through pinhole (1 mm) located at 15 mm downstream from reactor inlet. Exposure time of ICCD camera was 100 ms. Experimental system except optical setting was placed in a constant temperature bath where temperature was maintained at 120 °C to avoid liquid condensation. Detailed experimental condition is listed in Table 1.

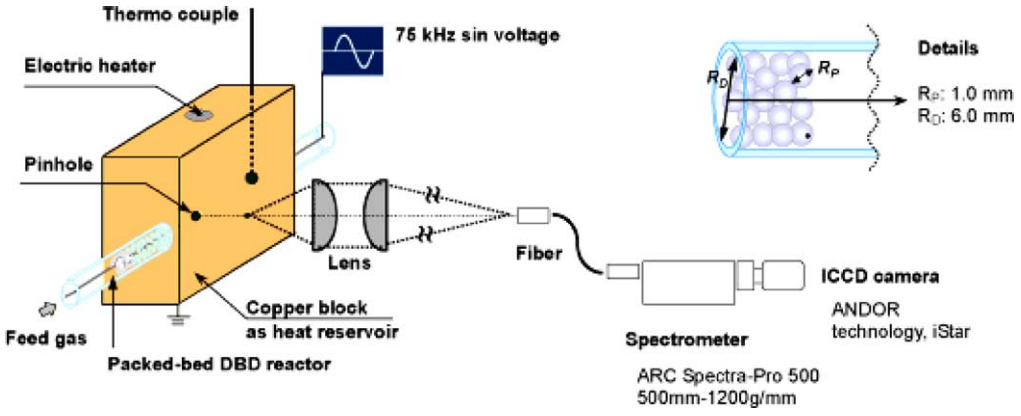

Fig. 2. Optical setup and reactor configuration.

4. Emission spectroscopy

4.1. Rotational temperature

Rotational temperature sufficiently reflects gas temperature where most chemical and electric processes take place. Fig. 3(B)–(D) shows simulated CH($A^2\Delta$) band spectrum that consists of three different vibrational components. Rotational and vibrational temperatures were assumed to be 423 and 5000, 10 000 and 15 000 K, respectively. Relative emission intensity for $v(0,0)$ vibration spectrum is similar to that for $v(1,1)$ and closely overlapped each other. Emission intensity for $v(2, 2)$ vibration band is weaker than others, still we can identify unique band head near 432.5 nm. Fig. 3(A) shows emission spectrum due to $A^2\Delta \rightarrow X^2\Pi$ (431.5 nm) transition of CH($A^2\Delta$) observed at 200 °C of bed temperature. Rotational temperature can be determined from relative intensity ratio of individual R line of CH spectrum. Background spectrum must be substituted before measuring relative intensity of R branches. When I_{UL} is emission intensity of a single R branch of wave number v, then

$$I_{UL} \propto S_{UL} \nu_{UL}^4 \exp\left(-\frac{E_U hc}{kT_{rot}}\right) \quad (1)$$

Here, S_{UL} is the line strength, ν_{UL} the wave number (cm^{-1}), E the rotational term (m^{-1}), k the Boltzmann constant (J/K), h the Planck's constant (J/s), c the velocity of light (m/s), T_{rot} the rotational temperature (K), and subscripts U and L denote upper and lower electronic states. The logarithmic plot of $\ln(I_{UL}) - \ln(S_{UL}\nu_{UL}^4)$ against $E_U hc/k$ is called Boltzmann plot and will provide a straight line when rotational state of excited CH($A^2\Delta$) established equilibrium with respect to translational gas temperature: gas temperature can be derived from given slope of Boltzmann plot (Fig. 4). Detailed numerical procedure to derive rotational temperature from measured data and reliability of measurement has been extensively investigated by Nozaki et al. [5–7].

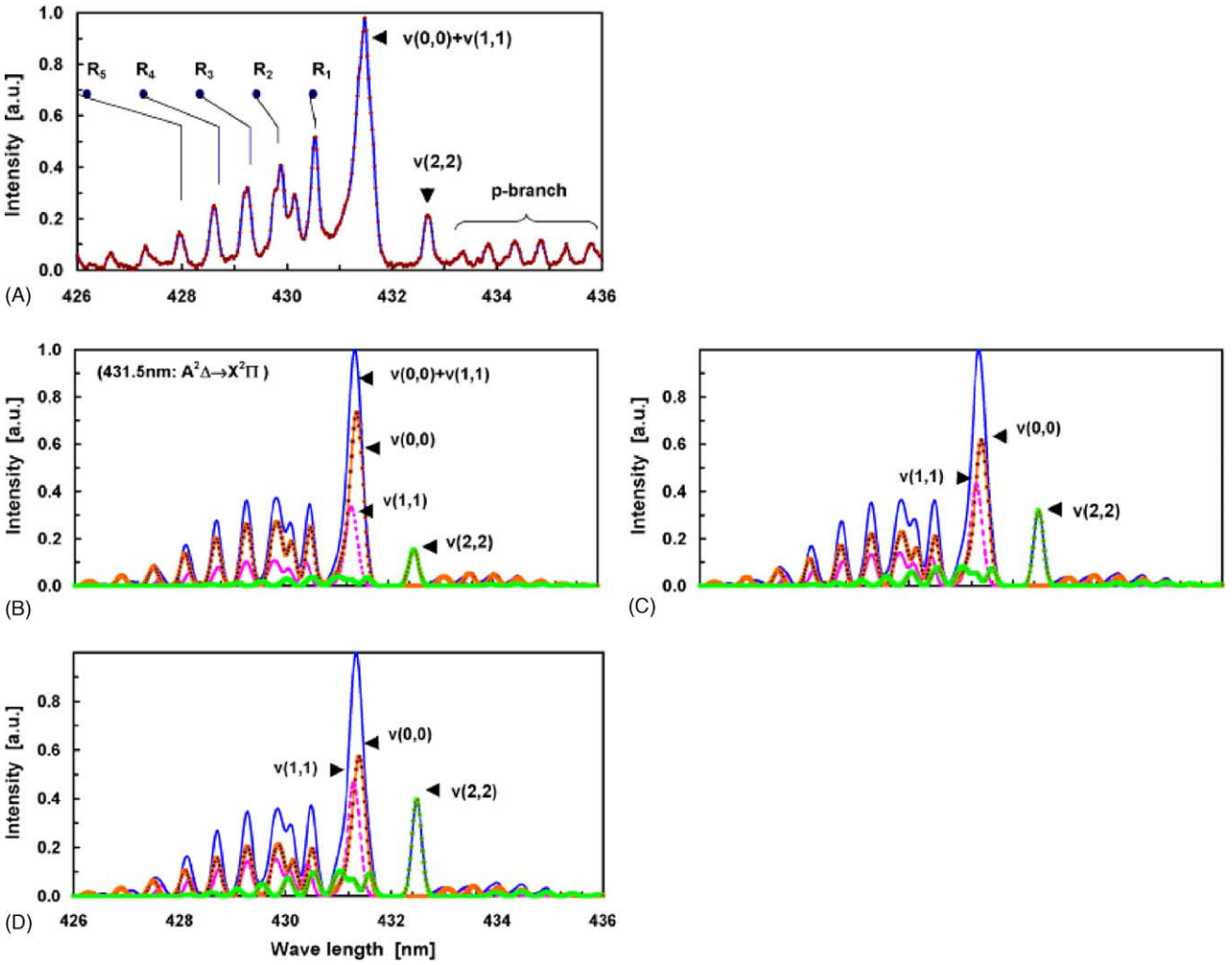

Fig. 3. Emission spectra for CH (431.5 nm: $A^2\Delta \rightarrow X^2\Pi$). (A) measured spectrum. Rotational temperature is 423 K, and vibrational temperature is (B) 5000 K, (C) 10 000 K, and (D) 15 000 K, respectively.

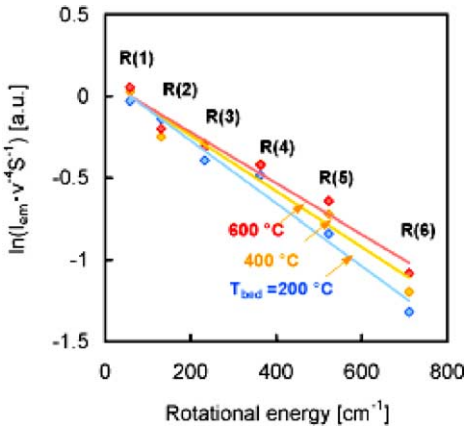

Fig. 4. Boltzmann plot.

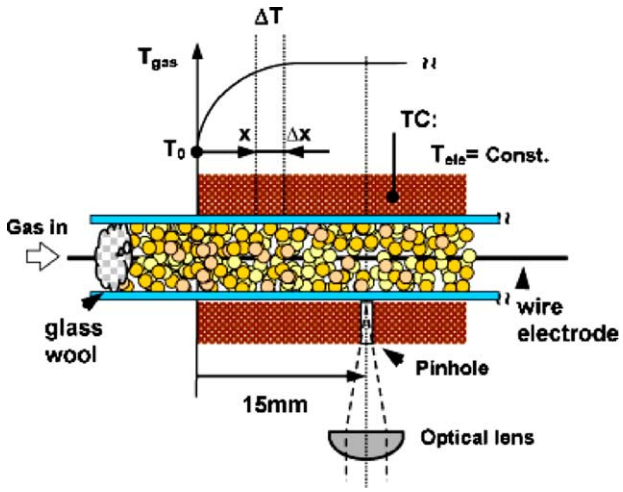

Fig. 5. Schematic diagram showing gas temperature evolution within packed-bed reactor.

4.2. Apparent vibrational temperature

On the other hand, we were not able to make sure whether vibrational state satisfactorily established equilibrium state because individual vibrational spectrum is closely overlapped. Observed emission spectrum corresponds to a sum of $v(0, 0)$, $v(1, 1)$, and $v(2, 2)$ as shown in Fig. 3. However, band head peak intensity for $v(2, 2)$ can be uniquely identified. Fig. 3(B)–(D) indicates that relative intensity ratio for $v(2, 2)$ and $v(0, 0) + v(1, 1)$ increases with vibrational temperature, whereas R branches that reflect rotational temperature is unchanged. From this point, apparent vibrational temperature was derived by fitting experimental and numerical intensity ratio with the following formula.

$$I'_v = \frac{I'_{v22}}{I'_{v00} + I'_{v11}}, \text{ and then}$$

$$I'_v \Big|_{\text{measurement}}^{\text{non-equillibrium}} \approx I_v \Big|_{\text{calculation}}^{\text{equilibrium}} \quad (2)$$

5. Gas temperature distribution in packed-bed reactor

Temperature distribution of flowing gas mixture in packed-bed reactor was calculated with the empirical formula by assuming constant bed temperature. Fig. 5 schematically illustrates reactor configuration and gas temperature evolution. Heat transfer between gas mixture and bed media is expressed by the following formulae [8].

$$\Delta Q = h_{\text{loc}}(aS\Delta x)(T_{\text{bed}} - T_{\text{gas}})\,[W] \quad (3)$$

Here, ΔQ is the heat flow between bed and gas media (W), h_{loc} the local heat transfer coefficient (W/m^2 K), a the pellet surface area per unit bed volume (m^{-1}), $S\Delta x$ the bed volume (m^3), T_{bed} the bed temperature (°C), and T_{gas} is the bulk gas temperature (°C). Gas temperature distribution also depends on heat generated by barrier discharges, thus gas temperature increase within small length Δx is expressed by

$$\Delta T = \frac{\Delta Q + GS\Delta x}{wC_{\text{pb}}}\,[\text{K}] \quad (4)$$

Here, ΔT is the bulk gas temperature deference over distance Δx (°C), G the uniform heat generation rate associated with power density of plasma (W/m^3), $w$the mass flow rate (kg/s), and C_{pb} is the specific heat of gas mixture evaluated at bulk gas temperature (J/(kg K)). Energy spent by barrier discharge is considered as uniform heat generation within packed-bed reactor. Heat absorption due to steam reforming underestimated heat generation rate, but it was no larger than 5% in this experiment. Therefore, we did not take into account of it for simplicity. A large amount of experiments provided empirical correlations for heat transfer coefficient in packed-bed media [8].

$$j_{\text{H}} = 0.91Re^{-0.51}, \quad \psi = \frac{h_{\text{loc}}}{C_{\text{pb}}u_0}\left(\frac{C_{\text{p}}\mu}{k}\right)^{2/3}_{\text{f}} \quad (Re < 50) \quad (5)$$

$$Re = \frac{u_0}{a\mu_{\text{f}}\psi}, \quad T_{\text{f}} = \frac{1}{2}(T_{\text{wall}} + T_{\text{gas}}), \quad u_0 = \frac{w}{S} = \rho u \quad (6)$$

Here, j_{H} is the Colburn j factor, Re the Reynolds number, ψ the empirical coefficient that depends on pellet shape (sphere takes unity), k the thermal conductivity of gas mixture (W/(m K)), μ the viscosity (kg/(m s)), u_0 the superficial mass velocity (kg/(m^2 s)), and subscript ‘f’ is the properties evaluated at the film temperature (T_{f}). Gas temperature distribution was calculated with those equations, and then compared to rotational temperature for consistent analysis.

6. Results and discussion

We first discuss on two-temperature analysis of BEC reactor for better understanding of reaction mechanism. Table 2 summarizes five different temperatures we obtained. Here, T_{bed} is the catalyst bed temperature measured with

Table 2
Relation among five different temperatures

Bed temperature (T_{bed}) ≈ electrode temperature (T_{ele})	200	400	600
Gas phase			
Empirical correlation (T_{gas})	507	642	793
Rotational temperature (T_{rot})			
SiO_2	466	575	648
Ni/SiO_2	430	555	628
Vibrational temperature (T_{vib})			
SiO_2	5026	5178	5600
Ni/SiO_2	5440	6610	12975

Gas phase temperatures were obtained at 15 mm down stream from the reactor inlet (°C).

thermocouple, T_{ele} the grounded electrode temperature with thermocouple, T_{rot} the rotational temperature determined from CH emission, and T_{gas} is the gas temperature calculated with empirical correlation. We could reasonably assume that $T_{bed} \approx T_{ele}$ and $T_{gas} \approx T_{rot}$ as discussed later, and then derived some of the important aspects for reaction mechanism. Finally, reactivity of vibrationally excited methane is discussed based on vibrational temperature (T_{vib}) of CH.

6.1. Verification of empirical correlation (Eqs. (3)–(6))

Fig. 6 compares temperature of ground electrode (T_{ele}) and bed temperature (T_{bed}) measured by thermocouple which was directly inserted into the bed media. Barrier discharge was turned off during the measurement. Bed temperature reached electrode temperature after steady-state was established. Although actual bed temperature was not able to measure when barrier discharge was turned on, we could satisfactorily assume that T_{ele} equals to T_{bed} from Fig. 6.

Fig. 7 shows gas temperature distribution in bed media calculated with empirical correlation by setting $G = 0$ (W/m^3) (Eq. (4)). The electrode temperature (T_{ele}) was 200 °C. The temperature was normalized by the following

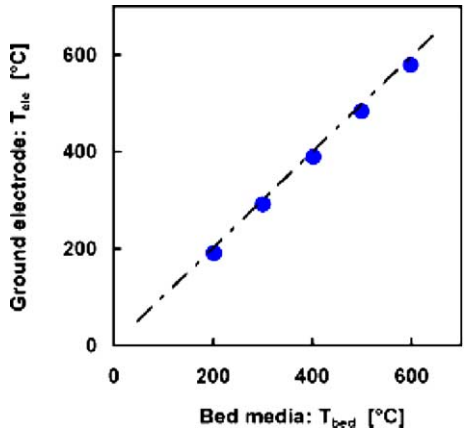

Fig. 6. Comparison between electrode temperature (T_{ele}) and bed temperature (T_{bed}). Both temperatures were measured by a thermocouple at 15 mm downstream from the inlet.

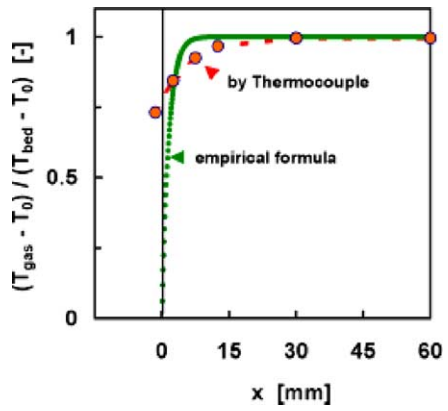

Fig. 7. Comparison between gas temperature distribution (line: empirical correlation) and bed temperature (solid symbol: measurement). Plasma was turned off (i.e. $G = 0$ W/m^3). Gas flow rate was 180 sccm and T_{bed} was 200 °C, respectively.

equation.

$$\theta = \frac{T_{gas} - T_0}{T_{bed} - T_0} \quad (7)$$

Here, T_0 is the initial gas temperature and set to 120 °C. When T_{bed} equals to T_{gas}, normalized temperature (θ) becomes unity. T_{gas} rapidly increases by heat transfer from high temperature bed media, and then it reaches T_{bed} within 7 mm downstream from the inlet. The actual bed temperature showed a similar profile, but it is slightly broadened because of heat conduction through bed media towards the upstream; however, Eq. (3) predicts gas temperature within acceptable error after 15 mm downstream from the inlet. From this point, we made a pinhole at this location for optical measurement as shown in Fig. 2.

6.2. Plasma gas temperature determined by rotational temperature

Rotational temperature, which reflects gas temperature inside filamentary discharges, is plotted in Fig. 8 with respect to bed temperature with/without nickel catalyst. Here, we

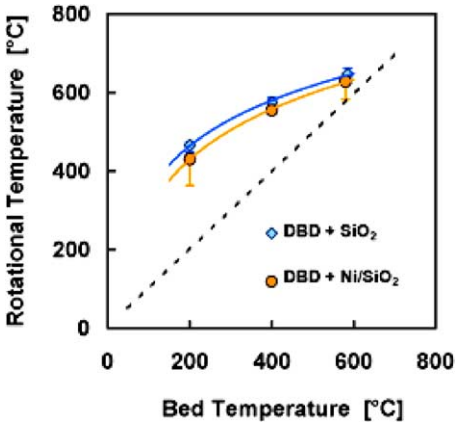

Fig. 8. Rotational temperature vs. bed temperature.

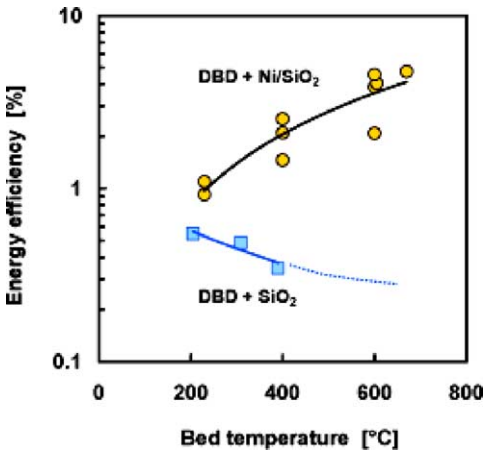

Fig. 9. Energy efficiency of BEC reactor operated at 76 kHz.

assumed $T_{bed} = T_{ele}$ from the previous discussion. Rotational temperature was elevated much higher than bed temperature when $T_{bed} = 200\,^{\circ}C$, while it gradually approached bed temperature until $T_{bed} = 600\,^{\circ}C$. Fig. 9 shows energy efficiency for BEC reactor expressed by the following formula.

$$\frac{\Delta H_{reform}}{W} \times 100\,(\%) \tag{8}$$

Here, ΔH_{reform} is the endothermic reaction enthalpy due to steam reforming. In the presence of nickel catalyst, 5% of discharge power was absorbed by reforming reaction at 600 °C; however, this effect was virtually negligible from the fact that rotational temperature was unchanged in spite of the existence of nickel catalyst.

Fig. 10 compares the calculated gas temperature (T_{gas}) distribution and rotational temperature (T_{rot}). Bed temperature was assumed to be uniform, and heat generation per unit volume in Eq. (4) was derived from power consumption by barrier discharge ($G \neq 0$). Gas temperature (T_{gas}) overestimated rotational temperature by 10–20% because Eq. (4) does not take into account heat conduction through bed media, but both temperatures showed similar dependence on bed temperature. From this point, we can conclude that rotational temperature represents gas temperature within acceptable error and provides reliable data. The calculation was also performed by considering heat absorption by reforming. The result showed that corresponding temperature dropped was about 8 °C when bed temperature was 600 °C. Actual temperature drop associated with steam reforming was too small to be detected with enough accuracy in the present set-up.

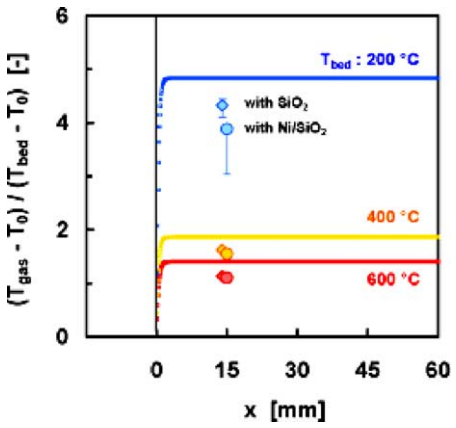

Fig. 10. Rotational temperature vs. calculated gas temperature by empirical correlation. Bed temperature was assumed to be constant. Discharge power was 35 W and total flow rate was 26 sccm.

These results imply more important aspects about plasma–catalyst interaction. Generally, rotational temperature exceeds much higher than average gas temperature because heat generated by streamers is localized in filamentary narrow regions. Nozaki et al. measured gas temperature distribution between two parallel-plate barrier discharge electrodes [7]. The gas temperature increase due to streamer formation reached 200 °C, while average gas temperature was increased only 30 °C. The gas temperature in the middle of gas gap was significantly increased with increasing input power because of poor cooling condition. On the contrary, in the packed-bed reactor, average gas temperature (T_{gas}) exceeded rotational temperature (T_{rot}). One reason is that Eq. (4) does not consider heat loss through bed media, thus T_{gas} overestimated actual plasma gas temperature. More importantly, streamer propagates along pellet surface, therefore efficient heat exchange from streamers to pellets is anticipated. This fact also means that interaction between streamer and catalyst is so effective that synergistic effect is readily available, even though void fraction of catalyst bed was 80%. Also, heat generated by streamer does not act as hot spot, which may unexpectedly promote steam reforming by thermal reaction at given electrode temperature. It is interesting to note that synergistic effect was not observed when $T_{bed} = 200\,^{\circ}C$, even though gas temperature reached as high as 500 °C. Catalyst bed temperature must be appropriately increased for deriving synergistic effect.

6.3. Reactivity of vibrationally excited $CH(^2\Delta)$

Computer modeling for streamer development in pure methane indicated that most abundant and long-lived radical species would be vibrationally excited methane: stretching mode (0.36 eV) and bending mode (0.16 eV). Creation of such species consumes 40% discharge power, and number density reaches 100 times higher than electron density ($N_e \sim 10^{14}\,cc^{-1}$). Generally, vibrational methane cannot contribute to chemical reaction because of their low reactivity. Inelastic electron collision to produce vibrational methane is therefore considered to be a major energy loss process. On the other hand, methane conversion was almost doubled in the presence of nickel catalyst without increasing discharge power; methane conversion exceeded much higher than equilibrium conversion, whereas products selectivity tended to follow equilibrium composition at given temperature. Decomposition of vibrationally excited methane on nickel catalyst is strongly anticipated to explain this drastic

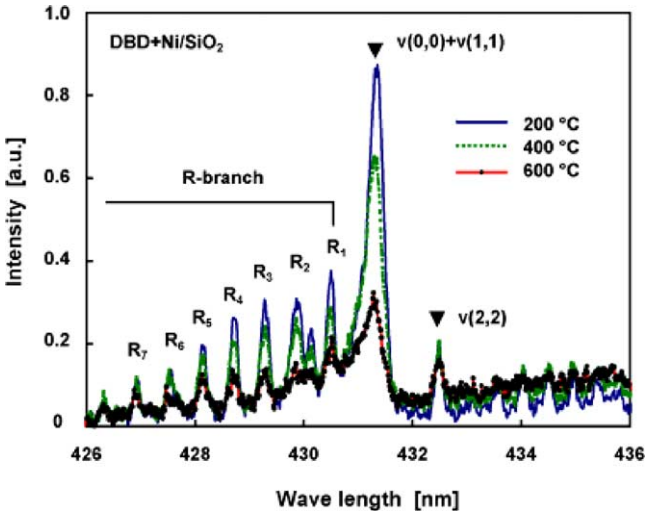

Fig. 11. Emission spectra of CH measured at different bed temperatures.

increase in methane conversion. In fact, vibrationally excited methane is able to promote dissociative chemisorption on nickel surface. In this section, we analyzed vibrational temperature of CH to explain the synergistic effect in BEC reactor.

Fig. 11 shows CH band spectra observed at different bed temperatures with nickel catalyst. The relative intensity of $v(2, 2)$ was clearly independent of bed temperature. On the other hand, combined intensity of $v(0, 0) + v(1, 1)$ significantly decreases with increasing bed temperature. This situation resulted in apparently higher vibrational temperature since relative intensity ratio expressed by Eq. (2) increases with bed temperature. Fig. 12 shows vibrational temperature of CH measured in BEC reactor with/without nickel catalyst. Vibrational temperature were independent of bed temperature in the absence of nickel catalyst; however, it significantly increased with nickel catalyst. As previously discussed, electric and optical properties such as reduced field strength, average electron density, and rotational temperature was not influenced by the presence of nickel catalyst [2]. This fact indicates that vibrationally excited

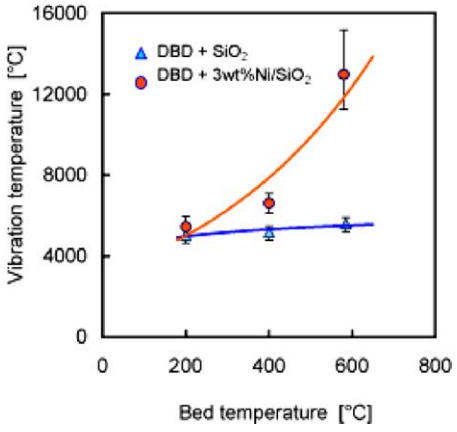

Fig. 12. Rotational temperature vs. bed temperature.

Table 3
Rotational relaxation due to $CH(A^2\Delta)$–CH_4 collisions during radiative lifetime of $CH(A^2\Delta)$

Gas temperature (°C)	Radiative lifetime (ns)	Collision frequency
127	2.7	36
427	4.8	47

Note: Collision number is 25.

methane at $v(0, 0)$ and $v(1, 1)$ states of $CH(A^2\Delta)$ was selectively reacted on nickel surface within radiative lifetime of $CH(^2\Delta)$.

The effective radiative lifetime of $CH(^2\Delta)$ in methane is derived as 2.7–4.8 ns from the quenching coefficient presented by Nokes and Donovan [9], and 35–50 collisions expected during radiative lifetime as summarized in Table 3. The number of collisions necessary to establish rotational equilibrium of $CH(^2\Delta)$, i.e. collision number, can be estimated with the formulae given by Widom [10], resulting in 25 collision number at given conditions. From this point, rotational state of $CH(^2\Delta)$ obviously reached equilibrium state within radiative lifetime, and provided similar intensity distribution of *R* branches almost independently of the presence of nickel catalyst as shown in Fig. 8. On the other hand, it is difficult to estimate relaxation of vibrational state because vibrational transition probability of $CH(^2\Delta)$ is not known. Generally, vibrationally excited molecule requires large number of molecular collision to establish vibrational equilibrium. This means that results presented in Fig. 12 shows "apparent" vibrational temperature. However, vibrational states of $CH(^2\Delta)\{v(0, 0)$ and $v(1, 1)\}$ are obviously affected by nickel catalyst within radiative lifetime of $CH(^2\Delta)$. It is quite possible that vibrationally excited CH reacted on nickel catalyst efficiently, thus emission intensity was significantly decreased with bed temperature. Increased reactivity of vibrationally excited methane on nickel catalyst is highly expected.

7. Conclusions

Rotational temperature of $CH(A^2\Delta)$ (T_{rot}), gas temperature (T_{gas}), and bed temperature (T_{bed}) in BEC reactor were individually analyzed for better understanding of reaction mechanism. In addition, reactivity of vibrationally excited methane was discussed based on vibrational temperature of $CH(A^2\Delta)$. Barrier discharge is recognized as non-equilibrium plasma from the fact that electron temperature (1–10 eV $\approx$ 104–105 K) is much higher than gas temperature (typically near room temperature). However, chemical conversion process depends largely on gas temperature (300–1000 K) as discussed in this paper. The non-equilibrium nature of barrier discharge, which is the most important feature of this kind of plasma sources, tended to be weakened with increasing gas temperature. Up to now authors are not able to make reasonably definition,

but it is definitely important to specify "the degree of non-equilibrium" quantitatively for better characterization of given plasma conversion processes. Some of the important aspects are as follows.

1. Gas temperature decrease due to steam reforming was not clearly detected: maximum endothermic enthalpy was not larger than 5% of the discharge power in this set-up, and empirical correlation predicted that average gas temperature would decrease by 8 °C.
2. Even though plasma gas temperature reached 400–500 °C, synergistic effect could not be expected when catalyst bed temperature was below 200 °C. Bed temperature must be maintained at a certain level independently of plasma gas temperature. This fact also means that heat produced by filamentary discharges does not act as hot spots.
3. Streamers propagate in close contact with pellet surface, therefore efficient heat exchange from streamers to pellets is anticipated. It also means that interaction between streamer and catalyst is so effective that synergistic effect is readily available, even though void fraction of catalyst bed was 80%.
4. Rotational temperature was independent of the presence of nickel catalyst. In addition, rotational equilibrium of excited CH($A^2\Delta$) is sufficiently established within radiative lifetime (2–3 ns).
5. Apparent vibrational temperature of CH significantly increased with respect to bed temperature only when nickel catalyst existed. On the other hand, it was independent of bed temperature in the absence of nickel catalyst. Vibrationally excited CH($A^2\Delta$) $\{v(0, 0)$ and $v(1, 1)\}$ was effectively reacted on nickel catalyst within radiative lifetime. Reaction enhancement in barrier discharge combined catalyst bed reactor was confirmed.

Acknowledgements

This research was partly supported by the Ministry of Education, Science, Sports and Culture, Grant-in-Aid for Young Scientists (B), 14750132, 2002, and The Mizuho Science Foundation. Authors also would like to thank Prof. M Suzuki, Associate Prof. H Akatsuka, Associate Prof. T Watanabe, and Associate Prof. Y. Kato (Tokyo Institute of Technology) for intensive discussion.

References

[1] L.B.F. Juurlink, P.R. McCabe, R.R. Smith, C.L. DiCologero, A.L. Utz, Phys. Rev. Lett. 83 (4) (1999) 868–871.
[2] T. Nozaki, N. Muto, S. Kado, K. Okazaki, Dissociation of vibrationally excited methane on Ni catalyst. Part 1. Application to methane steam reforming, Catal. Today, in print.
[3] C.T. Ceyer, J.D. Beckerle, M.B. Lee, S.L. Tang, Q.Y. Yang, M.A. Hines, J. Vac. Sci. Technol. A 5 (4) (1987) 501–507.
[4] H. Burghgraef, A.P. Jansen, R.A. van Santen, J. Chem. Soc. 101 (12) (1994) 11012–11020.
[5] T. Nozaki, Y. Unno, Y. Miyazaki, K. Okazaki, J. Phys. D: Appl. Phys. 34 (16) (2001) 2504–2511.
[6] T. Nozaki, Y. Miyazaki, Y. Unno, K. Okazaki, J. Phys. D: Appl. Phys. 34 (23) (2001) 3383–3390.
[7] T. Nozaki, Y. Unno, K. Okazaki, Plasma Sour. Sci. Technol. 11 (2002) 431–438.
[8] R. Byron Biurd, W.E. Stewart, E.N. Lightfoot, Transport Phenomena, International Edition, Wiley, New York, 1960.
[9] C.J. Nokes, R.J. Donovan, Chem. Phys. 90 (1984) 167–174.
[10] B. Widom, J. Chem. Phys. 32 (1960) 913–923.